Eur. Phys. J. B (2020) 93: 202
https://doi.org/10.1140/epjb/e2020-10367-y

THE EUROPEAN PHYSICAL JOURNAL B

Regular Article

The role of local bond-order at crystallization in a simple supercooled liquid

Søren Toxvaerd[a]

DNRF Centre "Glass and Time", IMFUFA, Department of Sciences, Roskilde University, Postbox 260, DK-4000 Roskilde, Denmark

Received 20 July 2020 / Received in final form 7 September 2020 / Accepted 9 September 2020
Published online 4 November 2020

Abstract. Large scale Molecular Dynamics simulations of 65 systems with $N = 80\,000$ Lennard–Jones particles at two different supercooled liquid state points reveal, that the supercooled states contain spatially heterogeneous distributed subdomains of particles with significant higher bond-order than the mean bond-order in the supercooled liquid. The onset of the crystallization starts in such an area with relatively high six-fold bond-order for a supercooled state, but low bond-order for a fcc crystal state, and the crystallization is initiated by a nucleus where all particles in the critical nucleus have a significant lower bond-order than in a fcc crystal. The critical nucleus of $N \approx 70$ particles is surrounded by many hundreds of particles with relatively high supercooled liquid bond-order and many of these particles are aligned with the crystal ordered particles in the critical nucleus. The crystallizations are very fast and supported by a fast growth of the supercooled areas with relative high liquid bond-order. The crystallizations are to fcc crystals, but a significant part of the crystallizations exhibit five-fold arrangements of polycrystalline subdomains mainly with fcc crystal order and sign of hcp crystallites.

1 Introduction

Computer simulations have allowed us to determine the dynamics of crystallization. Alder and Wainwright's [1] pioneering simulations of systems of hard spheres revealed, that a system of hard spheres at high packing fraction crystallizes into an ordered state with fcc lattice structure. Later, computer simulations of a system of particles with the more realistic Lennard–Jones (LJ) potential [2] not only confirmed the hard sphere result, but they were also in agreement with crystallizations of noble gases at low temperatures. Many later simulations of simple systems verified the result, that the minimum free energy of a condensed system of simple spherical symmetrical particles is for the fcc lattice arrangement [3–6].

The theory of crystallization is usually described by the classical nucleation theory (CNT) and its extensions [7–9]. But, an exact analyze [10] and many computer simulations of nucleation of liquids as well as crystals in supercooled gases exhibit a much more complex dynamics with polymorphism [11], then given by CNT. The critical nucleus in a gas phase is not a compact object of the new phase, and it is not only initiated by density fluctuations, but also by temperature fluctuations [12,13]. A recent review of theory and simulations of crystallizations is given in [14].

The supercooled liquid exhibits bond orientational order [15], and here we show that the bond-order, given by Q_6 [16], of the particles in a supercooled LJ liquid is heterogeneous distributed. The supercooled liquid contains big areas with significant higher bond-order than the mean bond-order in the liquid, and the crystallization is initiated from such an area. This result is consistent with the well known dynamic heterogeneities in supercooled liquids [17–19].

The crystallization is very fast and accompanied by a growth of the supercooled areas with relative high liquid bond-order. The growing crystal nuclei have fcc bond-order, but in many cases the nuclei also exhibit five-fold symmetry with polycrystalline domains. The crystalline domains are mainly with fcc crystal arrangements, but some are also with hcp structure. His behavior confirms previous results for homogeneous crystallizations in hard sphere systems [20,21] and in a LJ system [11,22–24]. Many of the polycrystalline nucleations ended in long time metastable polycrystalline states.

2 Homogeneous crystallization

Molecular dynamics (MD) systems of 80 000 LJ particles (see Appendices A and B) at different liquid state points were cooled down to the supercooled states (Fig. 1). We have performed 25 independent NVE simulations

[a] e-mail: st@ruc.dk

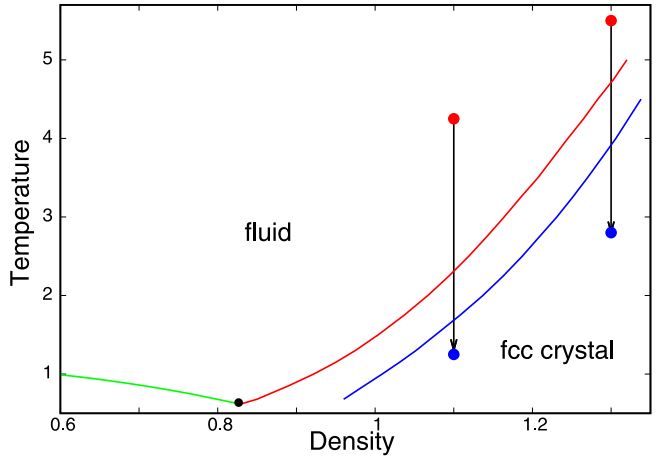

Fig. 1. The liquid–solid phase diagram for a LJ system. The liquid states, which coexist with gas are with light green. The liquid states, which coexist with solid fcc are red, and the coexisting fcc crystal states are blue. The MD systems are quenched from the liquids (red points) down to the supercooled liquids (blue points).

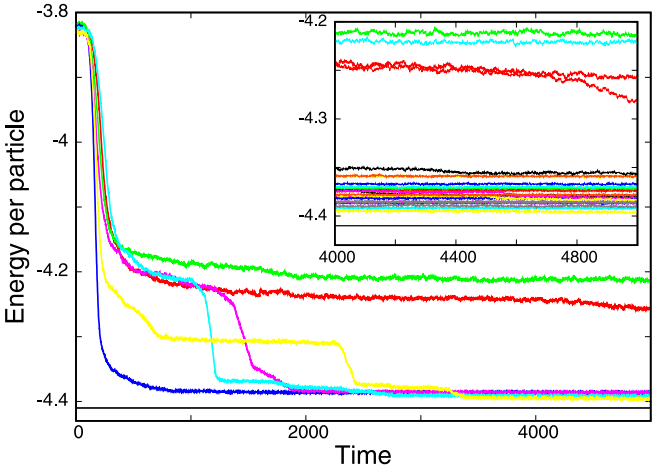

Fig. 2. Energy per particle, $u(t)$, as a function of the time after cooling to the supercooled state $(T, \rho) = (1.25, 1.10)$ (left blue point in Fig. 1). The figure shows six representative examples of $u(t)$. The inset are the energies for all 25 experiments in the time interval $\Delta t \in [4000, 5000]$ (i.e. for 1 million time steps after four million time steps). The black straight lines in the figure and the inset are the energy per particle for a perfect fcc crystal.

of supercooling and crystallizations at the state point $(T, \rho) = (1.25, 1.10)$, and 20 NVE and 20 NVT simulations at the state point $(T, \rho) = (2.80, 1.30)$. The degree of supercooling given by the ratio between the supercooled temperature T and the freezing point temperature of the liquid T_f is 0.54 and 0.60, respectively and the systems crystallized at the time $\Delta t \approx 50$–150 after the quenches. (Units are given in LJ units, see Appendix A, and the time unit $\Delta t = 1$ corresponds to 1000 MD time steps.)

The crystallizations result in a decrease in pressure and energy and were essentially completed within a crystallization time of $\Delta t \approx 50$. But for some of the simulations the crystallizations were, however, first completed after longer times. The energies per particle for the NVE crystallizations at $(T, \rho) = (1.25, 1.10)$ are shown in Figure 2, and the energies for the 20 NVT crystallizations are shown in Figure 9.

The description of the dynamics of the crystallization is divided into three subsections: the description of the supercooled liquid, the onset of crystallizations, and finally the crystallization and the description of the crystal states after the crystallizations were completed.

2.1 The supercooled liquid

The bond-order function Q_6 (defined in Appendix B) in the supercooled liquid is used to detect the dynamics of crystallization. The liquid state is characterized by having a low value of bond-order compared with the bond-order in the crystal state. In [25], the authors used bond-order in the Gaussian core model, which is a prototype for soft spheres, to analyze the onset of crystallization. They found, that the crystallization occurs in precursor regions of high bond orientation order, and that the crystal which first nucleates is the one which has the closest symmetry to the ordered regions in the supercooled state. A later investigation of the bond-order in a compressed hard sphere fluid found, however, that the hexagonal ordering appeared simultaneously with the density fluctuation at the onset of crystallization [26].

The present investigation shows, that the supercooled liquid contains large subregions of particles with relatively high Q_6 bond-order, and the nucleus which initiates the crystallization has only a bond-order which is somewhat higher than the order in the heterogeneous distributed bond-order domains, but on the other hand have a lower bond-order than in the crystal.

The distributions of the order parameter $Q_6(i)$ for particles i in the liquid state $(T, \rho) = (4.25, 1.10)$ (left red point) in Figure 1 and in the supercooled state $(T, \rho) = (1.25, 1.10)$ (blue point) are shown in Figure 3 together with the distribution in a fcc crystal state at $(T, \rho) = (1.25, 1.10)$. The distributions for the supercooled state (blue curve) and for the fcc crystal state (green curve) are separated, but the log distribution of $Q_6(i)$ in the inset of the figure reveals, that there is an exponential decreasing probabilities for low order in the crystal state and a high order in the supercooled state, and that there is an overlap of the two distributions in the region $0.35 < Q_6 < 0.45$. Investigation of the crystal ordering at the creation of the critical nucleus (next subsection) shows, that the successful nucleus have a mean order $Q_6 > 0.35$ in accordance with the distributions in Figure 3. The distributions of Q_6 for the liquid and the supercooled liquid, shown in Figure 3 are, however, different although they have the same mean Gaussian-like shapes. An analysis of the distribution of particles with relative high bond-order reveal this fact.

From the locations of particles with different values of $Q_6(i)$ for the particles i in the supercooled liquid one can see, that the distribution is non-uniform, and that there exists big subdomains with relative high values of

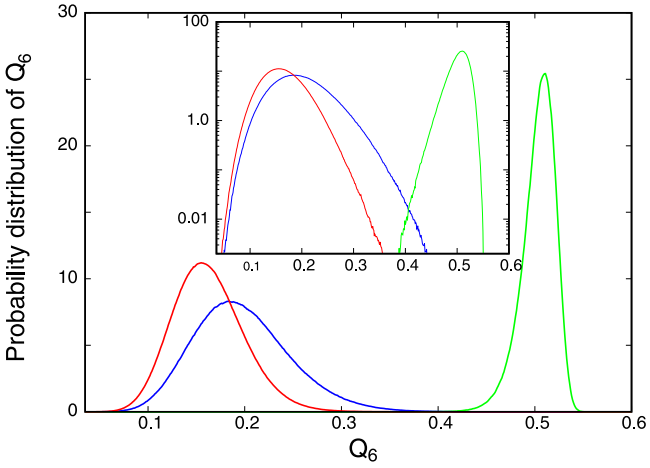

Fig. 3. Probability distribution of the bond-order parameter Q_6. The red curve is for the liquid before the cooling (left red point in Fig. 1) and the blue curve is for the supercooled liquid (left blue point in Fig. 1). The green curve is for a perfect fcc crystal at the supercooled state point. The inset shows the log-distributions.

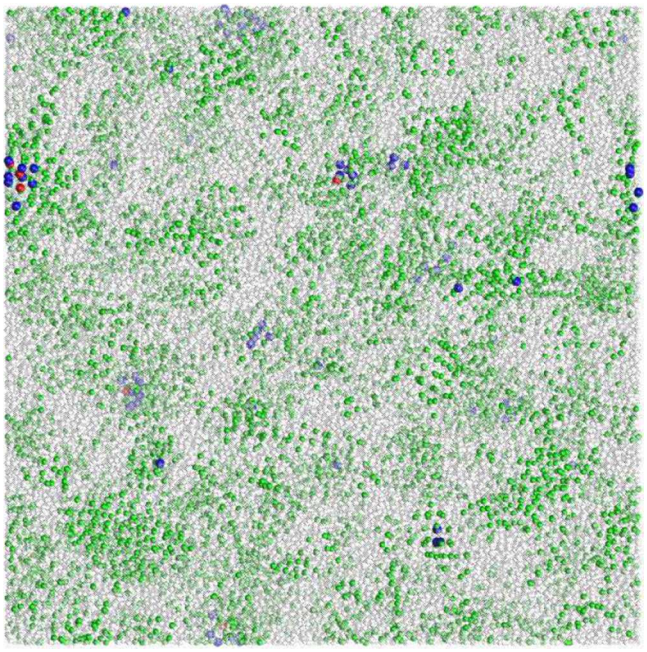

Fig. 4. Side view of the box with the N particles. The supercooled particles are colored accordingly to their bond-order, given by Q_6. Particles i with $Q_6(i) < 0.25$ are shown with white transparent. Green spheres: $0.25 < Q_6(i) < 0.35$; blue spheres: $0.35 < Q_6(i) < 0.40$; red spheres: $0.40 < Q_6(i)$.

$Q_6(i)$ for all the particles in the domain. The next figure shows this. Figure 4 is a side view of the positions at a certain time of particles i in the supercooled liquid. The white transparent spheres are particles with $Q_6(i) < 0.25$, green spheres have $0.25 < Q_6(i) < 0.35$, blue spheres have $0.35 < Q_6(i) < 0.40$, and the red spheres are particles in the supercooled liquid with a value of the bond-order $0.40 < Q_6(i)$. The blue and red particles are particles with a lattice order, which is sufficient for crystal nucleation. (The values of Q_6 are obtained as time averages over thousands time steps, but the heterogeneous distribution is also obtained from shorter and longer time intervals.) The positions of the particles is not uniformly distributed, but contains large areas with relative high bond-order.

The cluster distribution of particles in the system with a certain quality, e.g. a high Q_6 value, can be obtained directly during the MD simulation and without a significant increase in computer time for the big system by using the nearest neighbor list [12]. The clusters of N particles with $0.25 < Q_6(i)$ and the mean number n_N of clusters with N particles was determined directly during a MD simulation. The number $n_N(N)$, of a cluster with N particles with a bond-order $0.25 < Q_6$ within a time interval $\delta t = 0.1$ is shown in Figure 5. The value $Q_6(\mathbf{r}_i(t))$ of the bond-order for a particle i at position $\mathbf{r}_i(t)$ in the supercooled liquid state fluctuates with time, and the values of n_N in the figure are the mean for 200 independent distributions of clusters with $Q_6(i) > 0.25$, and where $Q_6(i)$ is obtained as the mean bond-order of a particle i within the time interval $\delta t = 0.1$ ($\approx$1 mean vibration within the shell of nearest neighbors). The figure shows the mean number n_N of clusters of N particles with relative high bond-order $Q_6(i)$ in the liquid state $(T, \rho) = (4.25, 1.10)$ (red curve) and the corresponding distribution of clusters in the supercooled state (blue curve). The two distributions are essentially different. The figure shows $\log(n_N)$ as a function of $\log(N)$ and the inset gives $\log(n_N)$ as

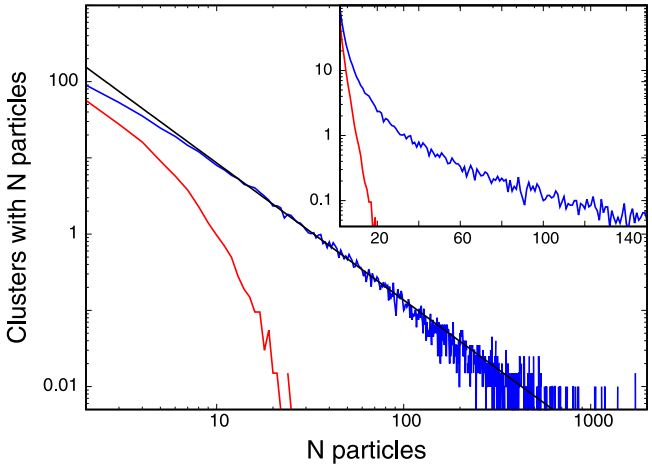

Fig. 5. Mean numbers of clusters n_N in the liquid states for clusters with N particles with bond-order $Q_6(i) > 0.25$ for all particles i in the clusters. The figure shows the $\log(n_N(\log(N))$ distributions and the inset is the $\log(n_N)(N)$ distributions. Red curves are for the liquid (left red point in Fig. 1) and blue curves are for the supercooled liquid. The straight black line in the figure is an algebraic fit, $a \times n_N^b$, to the distribution in the supercooled liquid for clusters in the interval $n_N \in [20, 200]$.

a function of N. The distribution in the liquid state is exponentially declining (red $\approx$ straight line in the inset), whereas the distribution for bigger clusters in the supercooled liquid is algebraic (blue $\approx$ linear function and black straight line in the figure). The black straight line is a line

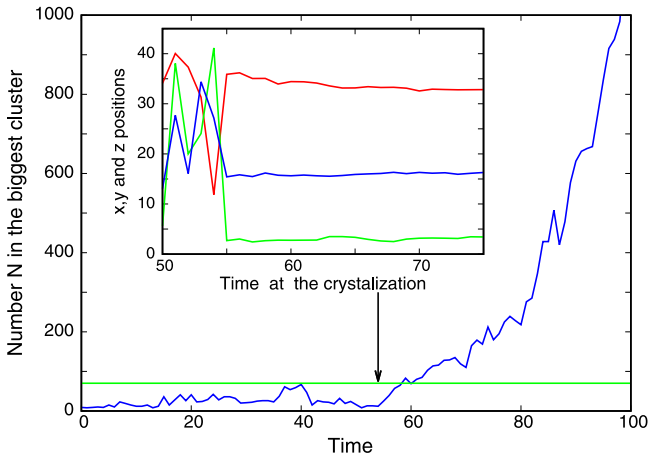

Fig. 6. Number $N(t)$, in 1 of the 25 simulations, of particles i in the biggest cluster of crystal-ordered particles with $0.35 < Q_6(i)$. The onset of crystallization at $t_{cr} = 56$ is marked by an arrow. From there the crystal nucleus grows quite monotonically. The green line is an estimate of the critical crystal cluster size of $N_{cr.} \approx 70$. The inset shows the x-, y-, and z-positions of the biggest cluster.

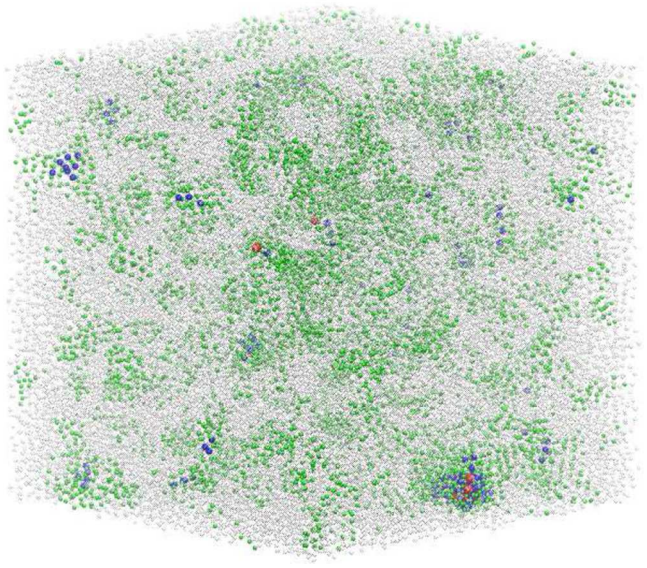

Fig. 7. The particle positions at $t = 0.58$ in the system with the $N(t)$ shown in the previous figure. The local environment with the critical nucleus is shown in the next figure. Color as in Figure 4.

obtained from a fit of $a \times N^b$ to the $\log(n_N(\log N))$ distribution in the interval $n_N \in [20, 200]$. The distribution of n_N shows also that there is regions of many particles, as can be seen in Figure 4, with relative high liquid bond-order $Q_6 > 0.25$.

The spatial algebraic- or "heterogeneous" distribution of particles with significant higher bond-order than the mean order in the supercooled liquid is consistent with the well-known dynamical heterogeneity in supercooled liquid [17–19]. In the next subsection, it is stated, that the crystallization is initiated in such a domain.

2.2 The onset of crystallization

The crystallization in a supercooled liquid appears when an ensemble of particles with lattice order gain free energy by increasing its size. In the CNT by, that the gain in free energy of the crystal phase exceeds the cost in surface free energy by the increased surface of the crystal. In the MD ensemble simulation, one primarily observes the crystallization, and the method gives not a direct information about the free energy. For this reason, it is not possible to determine the critical nucleus precisely. But one can locate the successful nucleus and its environment at the onset of nucleation.

The onset of crystallization is determined from the growth of the biggest cluster with bond-order $0.35 < Q_6$. In the supercooled liquid, the number N_c of particles in the biggest cluster with this crystal-like bond-order fluctuates with $N_c \leq 100$ (Fig. 6), but from the onset of crystallization the biggest cluster grows very fast, as shown in the figure. The x-, y-, and z- positions of the center of mass are shown in the inset. The time record of these positions identify the position of the successful nucleus even before it reaches the critical nucleus size. The rather constant location of the center of mass of the biggest cluster at times $t \geq 56$, and the fluctuating locations before $t = 56$ show, that different crystal-like nuclei appear in the system for $t < 56$, but from then on, the crystallization is initiated by this nucleus. The size of the successful nucleus at $t = 56$ is, however only $N_c = 17$ and clearly much smaller than the critical nucleus. But after only 2000 time steps, the center consists of 68 particles with $0.35 < Q_6$. The green line $N = 70$ is an estimate of the critical nucleus size, based on inspection of the 25 NVE simulation. As can be seen from Figure 6 some nuclei at times $t < 56$ before the crystallization sometime grow to this size. This behavior before the onset of nucleation is a typically for all 25 systems in the supercooled states.

The positions of the particles at $t = 58$ is shown in Figure 7 and with the same color as in Figure 4. The critical nucleus is enlarged in the next figure. Figure 8 shows the positions of the 574 particles within a sphere with the center at the center of mass of the critical nucleus and with the radius 5. The critical nucleus consists of 59 (blue) particles with $0.35 < Q_6 < 0.40$ and 9 (red) particles with $0.40 < Q_6 < 0.45$ (no particle have a $0.45 < Q_6$). There is 223 particles (green) with $0.25 < Q_6 < 0.35$ and the particles with $Q_6 < 0.25$ are white transparent. The mean bond-order of the 68 particles in the crystal-like critical nucleus is $\langle Q_6 \rangle = 0.38$. The green particles are mainly located in a shell around the critical nucleus and with a tendency to fit into the lattice planes of the critical nucleus. Even some of the white particles with lower bond-order are located in the critical crystals planes.

The crystal bond-order $\langle Q_6 \rangle$=0.38 in the critical nucleus is, however significantly lower than the bond-order in a bulk fcc crystal, and the twenty NVE and the twenty NVT simulations at the higher temperature and density

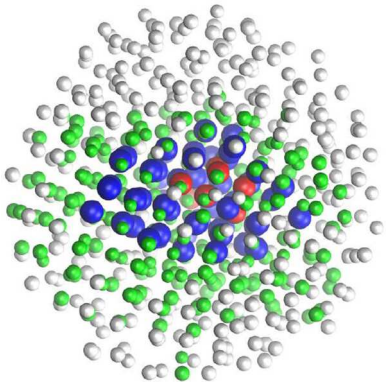

Fig. 8. The local environment of 574 particles within the sphere with radius 5 and with the center at the center of mass of the of the critical crystal nucleus shown in Figure 7. It consists of $N_c = 68$ particles with 59 (blue) particles with $0.35 < Q_6(i) < 0.40$ and 9 (red) particles with $0.40 < Q_6(i)$. The 225 small green particles have $0.25 < Q_6(i) < 0.35$ and the small white transparent part particles have $Q_6(i) < 0.25$.

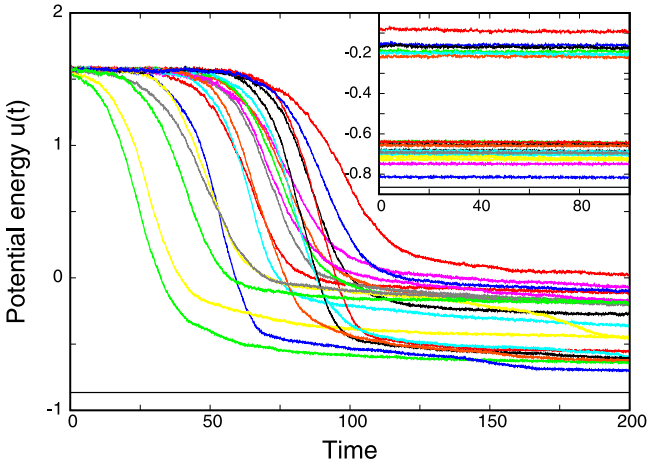

Fig. 9. Potential energy per particle, $u(t)$, as a function of time at the onset of crystallization for the $(T, \rho) = (2.80, 1.30)$ (right blue point in Fig. 1). The inset shows $u(t)$ at the end of the simulations.

$(T, \rho) = (2.40, 1.30)$ show the same tendency. All the critical crystal nuclei have a significant lower crystal Q_6 value than a perfect fcc crystals.

The means for the 25 crystal critical nucleus are:

Mean bond-order in the critical nucleus $\langle Q_6(i) \rangle = 0.38 \pm 0.02$, at the number of particles in the (estimated) critical crystal nuclei $N_{cr} = 73 \pm 4$.

In conclusion, the crystallization is initiated in a domain with excess bond-order for the supercooled liquid, but all the particles in critical nucleus have a bond-order significantly less than the bean bond-order in the crystal (fcc) state. This result disagrees with the result in [27] for homogeneous crystallizations in a system of hard ellipsoids.

2.3 The crystal states

Some crystallizations were completed within a short time-interval of 50–100 time units, but it took much longer times for many of the crystallizations as shown in Figure 2. Moreover, the systems did not end up in the same crystal state with energies close to the energy of a perfect fcc crystal. Some of the systems ended up in states with significant higher energies and pressures. For the 25 systems at the relative low density two to three of the simulations ended up in states with significant higher energies than the other systems. This tendency is more pronounced for the twenty NVE and the twenty NVT simulations at the higher temperature and density state $(T, \rho) = (2.80, 1.30)$.

Figure 9 shows the energy per particle $u(t)$ for the 20 NVT simulations after the supercooling, and with the energies at the end of the simulations in the inset of the figure. The energies exhibit two energy bands, with fourteen of the energies a little above the energy for a perfect fcc crystal (black line), whereas there are six simulations that have significant higher energies. The same result was obtained for the twenty NVE simulations at the same state point. From inspection of the particle positions and from the radial distribution functions, it is clear that the 14 systems in the lower energy band are fcc lattices with some defects, but the crystal states in the systems with energies in the upper energy band is more complex.

The structures of the systems with energies in the high energy band are investigated in order to determine their lattice structure. Particles interacting with simple spherical symmetrical pair-potentials can exist in many crystal arrangements [5]. But for a LJ system at the two-state point investigated here the fcc crystal structure has the lowest free energy [5,6]. The positions of particles for the system with the highest energy in Figure 9 (red upper energy function in the inset of Fig. 9) is shown in Figure 10. The particles are colored in accordance with their bond-order, and the colored positions show a complex crystalline structure with many areas with relative low bond-order and even without crystalline order ($Q_6 < 0.35$).

Crystalline order is traditionally determined from a systems structure factor or its Fourier transform, the radial distribution function $g(r)$. The extremes in the radial distribution functions at the high temperature $T = 2.80$ are, however, not sharp due the particles vibrations at their lattice positions. This thermal "noise" can be removed by cooling the system down to a low temperature. Figure 11 shows the radial distribution functions for the system with lowest energy (blue) and highest energy (red) in Figure 9, and the distribution $g_{\rm fcc}(r)$ for a perfect fcc lattice (green), and after the systems were cooled down to $T = 0.1$. The figure confirms, that both systems mainly consist of particles in a fcc arrangement. The disordered system with the highest energy deviates, however, from $g_{\rm fcc}(r)$ especially at the radial distance $r \approx 1.9$. The inset, where the two functions are compared with $g_{\rm hcp}(r)$ (green) for a hcp crystal reveals, that the crystal (Fig. 10) contains a small number of particles with hcp structure. The system with the highest energy was simulated over a very long time (47 000 time-units) in order to test whether it is stable, and it continued to be in the polycrystalline state.

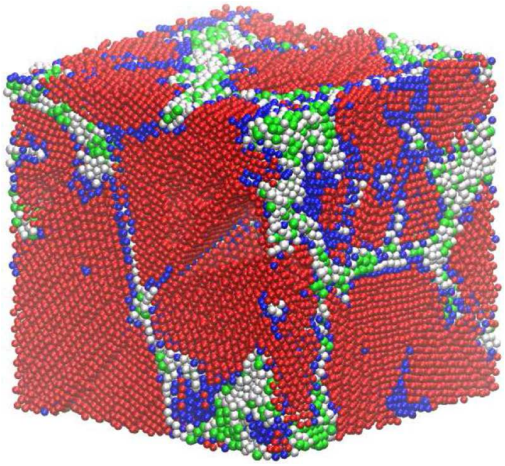

Fig. 10. Side view of the particles in the system with the highest energy after the crystallization (upper red curve in Fig. 9). The particles i are colored as in Figure 4. With: low order with $Q_6(i) < 0.20$: green $0.20 < Q_6(i) < 0.30$; blue: $0.30 < Q_6(i) < 0.45$; red: $0.45 < Q_6(i)$.

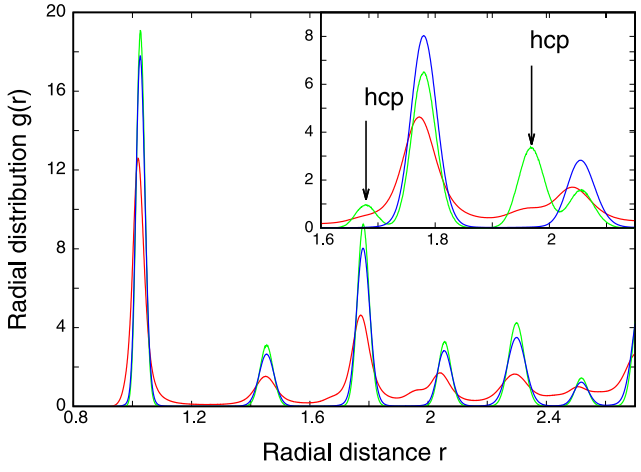

Fig. 11. The radial distribution functions for the system with the lowest energy (blue) and with the highest energy (red) in the twenty NVT simulations. After the crystallizations the systems were cooled down to $T = 0.1$ and compared with $g(r)$ for a perfect fcc crystal (green). The two distributions are compared with a corresponding hcp crystal distribution (green) in the inset.

The polycrystalline state is ensured in the beginning of the crystallization, and it is not a final size effect of the periodical boundaries. The next figure shows the particle positions 40 time-units after the onset of crystallization. The crystal nucleus consists of 5516 particles and the periodic plane in front goes through the crystalline nucleus and reveal, that the nucleus consists of several small crystals with different orientations of the crystal planes. The green particles in the supercooled liquid with relative high bond-order percolate the system and a new crystal center (upper left) is created with green particles included in the lattice arrangement. The figure shows that the spontaneous crystallization is preformed also by growing coherent order in the supercooled liquid (green particles), caused by the critical nucleus. This behavior of the spontaneous crystallization is found in all the crystallizations.

3 Conclusion

A supercooled liquid exhibits spatially heterogeneous dynamics [17], which influences the dynamic behavior of the supercooled and viscous liquid. Here it is determined, that the particles with relative high bond-order in the supercooled Lennard–Jones system is heterogeneous distributed, and that the supercooled liquid contains subdomains with significant higher bond-order than the mean bond-order in the supercooled liquid. Furthermore, the crystal nucleation is initiated from such region with relative high bond-order Q_6 for a supercooled liquid. The domains with excess bond-order changes in extension and locations with time, and this is "consistent" with the dynamic heterogeneities for supercooled liquid, but we have not directly established the connection between the domains of bond-order and the dynamics of the supercooled liquid, e.g. by determining the mobility of the particles in the subdomains.

The nucleus which initiates the crystallization is a relative compact object with six-fold symmetry as assumed in the classical nucleation theory (CNT), but all the $N \approx 70$ particles in the nucleus have, however, a significant smaller bond-order than the bond-order in the fcc crystal. And in addition, many of the surrounding particles in the subdomain are aligned with the particles in the initiating crystal nucleus (Fig. 8).

The growth of the critical nucleus is fast, and the crystal has percolate the big system of 80 000 LJ particles within a crystallization time of ≈50–100 time units. The systems did, however, not always end up in a homogeneous fcc state, but quite often they ended up in a polycrystalline state. The polycrystalline state with traces of hcp crystallites is, however, established in the crystal nucleus shortly after the onset of crystallization (Fig. 12). The polymorphism, where the particles crystallizes into different structures have already been observed in LJ systems [28,29]. Also here the areas with relative high bond-order in the supercooled part of the system plays a role for the fast-spontaneous crystallization. The heterogeneous distributed areas grow fast and percolate the system long times before crystallization.

The systems have been simulated by Molecular Dynamics NVE and NVT and with the same qualitative results. This is perhaps not surprising, because there is only a marginal difference between the two MD methods for the big system. This fact is due to, that the particles in the NVT dynamics are constrained to a thermostat temperature T_{th} by the excess of kinetic energy of the hole system. The systems mean temperature T in NVT are smoothly constrained over longer times to the $NVT's$ T_{th} value, which removes the latent heat during the spontaneous crystallization.

Ulf R. Pedersen, Trond S. Ingebrigtsen, and Jeppe C. Dyre are gratefully acknowledged. This work was supported by the VILLUM Foundation's Matter project, grant No. 16515.

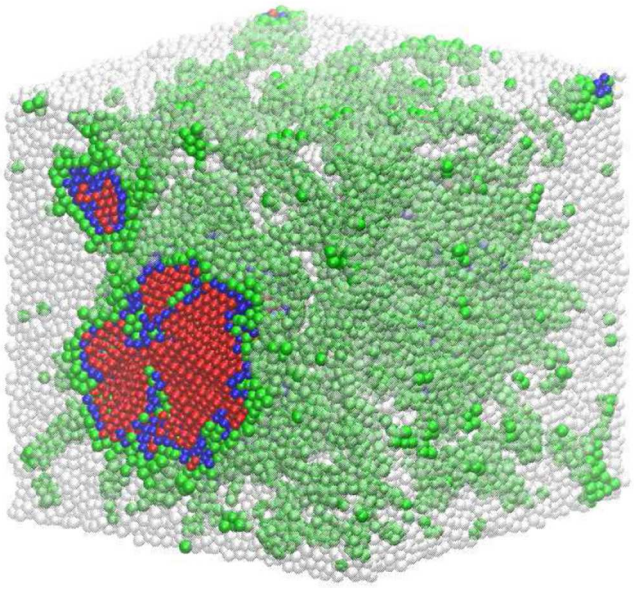

Fig. 12. Side view of the particles in the system (Fig. 10), but at a short time $\Delta t = 40$ after the onset of nucleation. The color of the spheres are the same as in Figure 10, but particles with $0.20 < Q_6$ are (white) transparent. The crystal cluster contains 5516 particles and the periodic boundary plane in front goes through the crystal nucleus.

Author contribution statement

The articles idea, programs used in the simulations, the simulations and the writing are done by the author.

Appendix A: The MD system and the computational details

The system consists of $N = 80\,000$ LJ particles in a cubic box with periodic boundaries, and the crystallizations are obtained by molecular dynamics NVE simulations with Newton's central difference algorithm [30] ("Leap-frog"). The time and length are given by the length unit $l^* = \sigma$ and energy unit $u^* = \epsilon/k_{\mathrm{B}}$ in the LJ potential for particles with the mass m. The unit of time is $t^* = \sigma\sqrt{m/\epsilon}$. The LJ forces are truncated and shifted at the interparticle distance $r_c = 2.5$ [31], by which the system is energy stable [32]. The molecular dynamics is performed with a small-time increment, $\delta t = 0.0010$ due to the high densities in the supercooled liquids.

The precise details of the phase diagram (Fig. 1) for a LJ system depends on, from where the long-range attractive forces are ignored, given by the value of r_c [33]. Most simulations of LJ systems including this one are for $r_c = 2.5$, for which the triple point densities are $(\rho_l, \rho_s, T) = (0.8290, 0.9333, 0.618)$ [34]. The present simulations of crystallizations are for supercooled liquids at the state points $(T, \rho) = (1.25, 1.10)$ and $(T, \rho) = (2.80, 1.30)$. The crystallizations can be characterized as crystallizations in supercooled condensed liquid states.

The crystallizations are performed by cooling from the liquid states at $(T, \rho) = (4.25,1.10)$ and $(T, \rho) = (5.25,1.30)$ down to the supercooled states $(T, \rho) = (1.25, 1.10)$ and $(T, \rho) = (2.80, 1.30)$, respectively. The cooling and NVT simulations are performed by a standard NVT thermostat. The NVE simulations are performed by cooling the high temperature system down in 10 000 time steps by the thermostat. The NVE supercooled state was accepted, if the temperature in the succeeding 10 000 time steps without a thermostat was within the temperature interval $T \in 1.25 \pm 0.005$. The temperature in the systems increases at crystallization for simulations without a thermostat. The NVE systems were, however, so supercooled, that they ended up in crystal states $(\mathrm{T},\ \rho) \leq (1.63, 1.10)$ with total crystallization. A LJ fcc crystal at $\rho = 1.1$ melts at $T = 1.68$ [35].

Appendix B: Identifying crystal structure

The crystal order is determined by a modified bond-orientation order analysis [16,25,36]. A complex order parameter

$$q_{lm}(i,t) \equiv 1/n_b \Sigma_{j=1}^{n_b} Y_{lm}(\mathbf{r}_{\alpha\beta}(t)) \tag{B.1}$$

is calculated for each particle i at time t. The sum over the n_b particles j in the local environment runs over all neighbors α of particle i plus the particle i itself [36]. A potential neighbor β to α is defined as a particle j within the first coordination shell of particle α, given by the first minimum in the radial distribution function. $\mathbf{r}_{\alpha\beta}(t)$ is the vector between a particle α in n_b and a nearest neighbor β. The summation is further restricted to the sum over no more than the twelve nearest neighbors [25] (there are occasionally more than twelve nearest neighbors in the first coordination shell in the supercooled liquid states). The Y_{lm} are the spherical harmonics, and the Steinhardt order parameter is defined as

$$Q_l(i,t) = \sqrt{\frac{4\pi}{2l+1} \Sigma_{m=-l}^{l} \mid q_{lm}(i,t) \mid^2}. \tag{B.2}$$

In [36], the authors compared Q_6 and Q_4 for different crystal structures. The present LJ system crystallizes into a fcc crystal, and the best separation between the bond-order in the supercooled liquid states and in the crystal states is obtained for Q_6 (Fig. 3). Finally, a temporarily stable crystal order at particle i is determined by averaging over a short time-interval of one time unit

$$Q_6(i) = \langle Q_6(i,t) \rangle. \tag{B.3}$$

The clusters of particles with crystal order are obtained directly during the simulations [12]. The threshold value for crystal order is $Q_6(i) \approx 0.35$ accordingly to Figure 3. A crystal nucleus is determined by, that all particles in

the nucleus have an order $Q_6(i) > 0.35$, and all particles in the nucleus have at least one nearest neighbor particle j with $Q_6(j) > 0.35$. The cluster distribution is obtained directly during the simulations. The biggest cluster is the successful nucleus, and the center of mass of the biggest nucleus reveal whether there is a competition between different growing crystals. It was never observed, once the successful nucleus was established (see inset in Fig. 6).

References

1. B.J. Alder, T.E. Wainwright, J. Chem. Phys. **27**, 1208 (1957)
2. J.P. Hansen, L. Verlet, Phys. Rev. **184**, 151 (1969)
3. S. Auer, D. Frenkel, Nature **409**, 1020 (2001)
4. S. Pronk, D. Frenkel, J. Chem. Phys. **110**, 4589 (1999)
5. J.C. Pámies, A. Cacciuto, D. Frenkel, J. Chem. Phys. **131**, 044514 (2009)
6. J.R. Errington, P.G. Debenedetti, S. Torquato, J. Chem. Phys. **118**, 2256 (2003)
7. M. Volmer, A. Weber, Z. Phys. Chem. **119**, 277 (1926)
8. R. Becker, W. Döring, Ann. Phys. (Leipzig) **24**, 719 (1935)
9. For a recent review of CNT, see V. Kalikmanov, *Nucleation Theory* (Springer, 2013)
10. A. Kuhnhold, H. Meyer, G. Amati, P. Pelagejcev, T. Schilling, Phys. Rev. E **100**, 052140 (2019)
11. W. Ouyang, B. Sun, Z. Sun, S. Xu, J. Chem. Phys. **152**, 054903 (2020)
12. S. Toxvaerd, J. Chem. Phys. **143**, 154705 (2015)
13. S. Toxvaerd, J. Chem. Phys. **144**, 164502 (2016)
14. S. Jungblut, C. Dellargo, Eur. Phys. J. E **39**, 77 (2016)
15. H.Tanaka, Eur. Phys. J. E **35**, 113 (2012)
16. P.J. Steinhardt, D.R. Nelson, M. Ronchetti, Phys. Rev. B **28**, 784 (1983)
17. M.D. Ediger, Ann. Rev. Phys. Chem. **51**, 99 (2000)
18. A. Widmer-Cooper, P. Harrowell, H. Fynewever, Phys. Rev. Lett. **93**, 135701 (2004)
19. A. Widmer-Cooper, P. Harrowell, Phys. Rev. Lett. **96**, 185701 (2006)
20. B. O'Malley, I. Snook, Phys. Rev. Lett. **90**, 085702 (2003)
21. N.C. Karayiannis, R. Malshe, M. Kröger, J.J. de Pablo, M. Laso, Soft Matter **8**, 844 (2012)
22. P.R. ten Wolde, M.J. Ruiz-Montero, D. Frenkel, Phys. Rev. Lett. **75**, 2714 (1995)
23. A.V. Anikeenko, N.N. Medvedev, J. Struct. Chem. **47**, 267 (2006)
24. C. Desgranges, J. Delhommelle, Phys. Rev. Lett. **98**, 235502 (2007)
25. J. Russo, H. Tanaka, Soft Matter **8**, 4206 (2012)
26. J.T. Berryman, M. Anwar, S. Dorosz, T. Schilling, J. Chem. Phys. **145**, 211901 (2016)
27. S. Dorosz, T. Schilling, J. Chem. Phys. **139**, 124508 (2013)
28. C. Desgranges, J. Delhommelle, J. Am. Chem. Soc. **128**, 10368 (2006)
29. C. Desgrange, J. Delhommelle, J. Phys. Chem. B **111**, 1465 (2007)
30. S. Toxvaerd, Eur. Phys. J. Plus **135**, 267 (2020)
31. S. Toxvaerd, J.C. Dyre, J. Chem. Phys. **134**, 081102 (2011)
32. S. Toxvaerd, O.J. Heilmann, J.C. Dyre, J. Chem. Phys. **136**, 224106 (2012)
33. S. Toxvaerd, Condens. Matter Phys. **18**, 13002 (2015)
34. S. Toxvaerd, J. Phys. Chem. C **111**, 15620 (2007)
35. M.A. Barroso, A.L. Ferreira, J. Chem Phys. **116**, 7145 (2002)
36. W. Lechner, C. Dellago, J. Chem. Phys. **129**, 114707 (2008)